

THE EFFECT OF ANGULAR STRUCTURE OF GAMMA-RAY BURST OUTFLOWS ON THE AFTERGLOW EMISSION

A. PANAITESCU AND P. KUMAR

Department of Astronomy, University of Texas, Austin, TX 78712

ABSTRACT

We investigate analytically the effect that an anisotropic kinetic energy distribution within a relativistic GRB fireball has on the decay of the afterglow emission, focusing on axially symmetric fireballs for which the energy outside a small uniform core is a power-law with the angle measured from the symmetry axis. The afterglow fall-off steepens after the core becomes visible to the observer. For observer directions within the core, simple formulae are derived for the power-law decay of the afterglow after the break, while for off-core observers the light-curve decay is shown graphically. Some criteria for assessing the effect of the outflow angular structure and collimation are given. Applying them to several GRB afterglows with light-curve breaks, we find that jets endowed with structure are required only if the circumburst medium has a wind-like (r^{-2}) stratification. However, numerical calculations of the synchrotron emission obtained for such external media suggest that the resulting light-curve steepening is too slow, most likely incompatible with the sharpness of the breaks observed in many afterglows. From numerical fits to the multiwavelength emission of the afterglows 990510 and 000301c, we find that, for the former, the ejecta kinetic energy did not vary by more than a factor ~ 3 across the jet surface, and that the sharp break of the R -band light-curve of the latter cannot be accommodated by a structured jet, re-enforcing our previous conclusion that it arose from the passage of a spectral feature through the optical domain.

Subject headings: gamma-rays: bursts - ISM: jets and outflows - methods: numerical - radiation mechanisms: non-thermal - shock waves

1. INTRODUCTION

Almost all the analysis of the decaying light-curves of Gamma-Ray Burst (GRB) afterglows is done within the framework of external shocks driven into the circumburst medium by ultrarelativistic ejecta (Mészáros & Rees 1997) whose kinetic energy is the same in all directions¹. A non-isotropic distribution of the energy per solid angle within the outflow is a natural extension of the afterglow model. Fireballs whose kinetic energy and initial Lorentz factor fall-off with angle are power-laws have been considered for the first time by Mészáros, Rees & Wijers (1998), who studied the effect of such distributions on the afterglow light-curve decay. Postnov, Prokhorov and Lipunov (2001) have suggested that GRB outflows may have a universal angular structure, the observed distribution of isotropic γ -ray outputs (which has a width of 3 dex) being due to the observer location. Rossi, Lazzati & Rees (2002) and Zhang & Mészáros (2002) have proposed that the light-curve breaks seen in several GRB afterglows and the narrow distribution of the GRB output and kinetic energies inferred by Frail et al. (2001) and Panaiteescu & Kumar (2002), respectively, may be due to the structure of fireballs.

In this work, we present an analytical treatment of the afterglow light-curves from structured fireballs (§2), with focus on axially symmetric fireballs endowed with a power-law distribution of the energy (§2.2). As we shall see, the initial distribution of the Lorentz factor is, most likely, irrelevant for current observations. In §3 we give a few criteria which, using the observed major features of afterglow light-curves, determine when the structure of fireballs is an important factor, and apply these criteria to study the best observed afterglows whose optical light-curves exhibited a break. Section §3.1 presents the numerical modeling of two GRB afterglows, 990510 and 000301c, in the

framework of structured jets, leading to a few important conclusions about the role of structure in these two cases.

2. ANALYTICAL CALCULATION OF AFTERGLOW LIGHT-CURVE DECAY

In this section we calculate the evolution of the afterglow light-curve index $\alpha(t)$, defined as the logarithmic derivative with respect to the observer time t of the received flux F_ν , for a fireball endowed with structure. Our aim is to obtain the dependence of the asymptotic values of α on the non-uniformity of the fireball, thus estimating the steepening of the light-curve decay that a fireball with structure can produce.

We consider ultra-relativistic ejecta (Lorentz factor $\gamma \gg 1$) whose kinetic energy per solid angle \mathcal{E} is axially symmetric, i.e. a function of only the angle θ measured from the symmetry axis of the fireball. The direction toward the observer (i.e. the fireball center–observer line) is at an angle θ_{obs} relative to this axis. The fireball dynamics and emission are calculated in spherical polar coordinates (δ, ψ) measured from the direction toward the observer, δ being the polar angle and ψ the azimuthal one, thus θ is related to (δ, ψ) through a rotation:

$$\cos \theta = \cos \delta \cos \theta_{obs} - \sin \delta \cos \psi \sin \theta_{obs} . \quad (1)$$

The calculation of the afterglow light-curve requires the following ingredients: dynamics of the fireball, spectrum of its emission, and integration over the equal photon-arrival-time surface. For analytical calculations, we shall ignore the tangential motions and mixing in the fireball and consider a simplified scenario where a patch $(d\delta, d\psi)$ travels as if it were part of a uniform fireball.

2.1. Synchrotron Emission from Structured Fireballs

¹Throughout this article, we use the term "uniform" to designate such outflows. If the angular distribution of the energy is not isotropic, the outflow will be called "structured". Tightly collimated outflows undergoing a significant lateral spreading at the time of observations will be referred to as "jets", while "fireballs" will be used if the lateral spreading is unimportant.

When afterglow observations are usually made, starting a few hours after the GRB, the fireball dynamics is nearly adiabatic. Thus the Lorentz factor γ of a $(d\delta, d\psi)$ patch decreases with its radial location r as:

$$\gamma = \Gamma \left(\frac{r}{r_d} \right)^{-(3-s)/2}, \quad (2)$$

in the relativistic regime $\gamma \gg 1$, where Γ is the initial Lorentz factor of the ejecta moving in the direction (δ, ψ) , $s = 0$ for a homogeneous medium (constant particle density n), $s = 2$ for a wind-like medium [$n(r) \propto r^{-2}$], and

$$r_d \propto (\mathcal{E}/\Gamma^2)^{1/(3-s)} \quad (3)$$

is the deceleration radius, up to which $\gamma \sim \Gamma$. The arrival-time t of photons emitted by the $(d\delta, d\psi)$ patch is given by integrating

$$dt = (dr/c)(1 - \beta \cos \delta), \quad (4)$$

where β is the velocity of the patch divided by the speed of light c . In the $\gamma \gg 1$ limit, using equation (2), one obtains

$$t = \frac{r}{c} \left[1 - \cos \delta + \frac{1}{2(4-s)} \left(\frac{r}{r_d} \right)^{3-s} \frac{\cos \delta}{\Gamma^2} \right], \quad (5)$$

at $r > r_d$. For $r < r_d$ the last term in the right-hand side sum above is just Γ^{-2} .

The synchrotron flux received by the observer at frequency ν is given by

$$F_\nu(t) \propto \int_\Omega \frac{d\Sigma}{[\gamma(1 - \beta \cos \delta)]^3} \mathcal{N} B \mathcal{F}(\nu, \nu_i) \quad (6)$$

where the integral is over all directions of ejecta motion, $d\Sigma = r^2 \sin \delta d\delta d\psi$ is the fireball surface element at location (r, δ, ψ) related to the observer time t through equation (5),

$$\mathcal{N} \propto r^{-2} \int_0^r n(r') r'^2 dr' \propto r^{1-s} \quad (7)$$

is the surface density of the electrons that have been energized by the shock sweeping-up the external medium,

$$B^2 \propto n \gamma^2 \propto r^{-s} \gamma^2 \quad (8)$$

is the magnetic field within the shocked fluid, and $\mathcal{F}(\nu, \nu_i)$ is the ratio of the flux at frequency ν and at the peak ν_i of the synchrotron spectrum of the fireball emission. Equation (6) simply states that the received spectral flux is the comoving frame synchrotron peak flux, proportional to $d\Sigma \mathcal{N} B$, relativistically beamed by the Doppler factor

$$\mathcal{D} = [\gamma(1 - \beta \cos \delta)]^{-1}, \quad (9)$$

taking into account the synchrotron spectrum $\mathcal{F}(\nu, \nu_i)$ of the emission. Thus, the flux integrated over the equal photon arrival time is

$$F_\nu(t) \propto \int_\Omega d\delta d\psi \sin \delta \frac{r^{3(1-0.5s)}}{\gamma^2(1 - \beta \cos \delta)^3} \mathcal{F}(\nu, \nu_i). \quad (10)$$

The spectral factor $\mathcal{F}(\nu, \nu_i)$ is determined by the distribution of the radiating electrons. This distribution is shaped by

the continuous injection in the downstream region of shock-accelerated electrons with a power-law distribution in energy, $dN_i/d\epsilon \propto \epsilon^{-p}$, above a minimum electron energy $\epsilon_i \propto \gamma$, and by radiative cooling. The resulting electron distribution exhibits a cooling break at an energy ϵ_c where the cooling timescale equals the age of the fireball, above which the effective electron distribution is $dN/d\epsilon(\epsilon > \epsilon_c) \propto \epsilon^{-(p+1)}$ if $\epsilon_c > \epsilon_i$ (e.g. Kardashev 1962), which is most likely the case for afterglow observations made a few hours after the burst. Consequently, the synchrotron spectrum is piecewise power-law, with breaks at the injection frequency $\nu_i \propto \mathcal{D} \epsilon_i^2 B$ and cooling frequency $\nu_c \propto \mathcal{D} \epsilon_c^2 B$:

$$\mathcal{F}(\nu, \nu_i) = \begin{cases} (\nu/\nu_i)^{1/3} & \nu < \nu_i \\ (\nu/\nu_i)^{-(p-1)/2} & \nu_i < \nu < \nu_c \\ (\nu/\nu_i)^{-p/2} (\nu_c/\nu_i)^{1/2} & \nu_c < \nu \end{cases}. \quad (11)$$

To obtain the dependence of the integrand in equation (10) on δ and ψ , i.e. on the fireball structure, we scale r and t to their values at the deceleration radius, defining $\rho \equiv r/r_d$, and

$$\tau \equiv t/t_d \propto \Gamma^{2(4-s)/(3-s)} \mathcal{E}^{-1/(3-s)} t, \quad (12)$$

where $t_d \equiv r_d/(2c\Gamma^2)$ would be the observer frame deceleration timescale if the fluid were moving directly toward the observer ($\delta = 0$). Therefore, equation (5) for $r(t)$ becomes

$$2(1 - \cos \delta) \Gamma^2 \rho + \frac{\cos \delta}{4-s} \rho^{4-s} = \tau, \quad (13)$$

for $\rho \ll \Gamma^{2/(3-s)}$, so that $\gamma \gg 1$ is ensured. With the aid of equations (2) and (3), the received flux (eq. [10]) is

$$F_\nu \propto \int_\Omega d\delta d\psi \sin \delta \frac{\mathcal{E}^{3(2-s)/2(3-s)}}{\Gamma^{(12-5s)/(3-s)}} \frac{\rho^{6-2.5s}}{(1 - \beta \cos \delta)^3} \mathcal{F}(\nu, \nu_i), \quad (14)$$

where $\mathcal{F}(\nu, \nu_i)$ is given by equation (11) with

$$\frac{\nu}{\nu_i} = \rho^{3-0.5s} \Gamma(1 - \beta \cos \delta) \frac{\nu}{\nu'_i(t_d)}, \quad \frac{\nu_c}{\nu_i} = \rho^4 \left[\frac{\nu_c}{\nu_i}(t_d) \right], \quad (15)$$

$\nu'_i(t_d)$ being the comoving frame injection frequency at the deceleration timescale, whose dependence on the fireball structure is

$$\nu'_i(t_d) \propto \Gamma^{(9-2s)/(3-s)} \mathcal{E}^{-s/2(3-s)}, \quad (16)$$

and

$$\frac{\nu_c}{\nu_i}(t_d) \propto \Gamma^{-8/(3-s)} \mathcal{E}^{2(s-1)/(3-s)}, \quad (17)$$

being the ratio of cooling and injection frequencies at t_d .

For a given fireball structure $\mathcal{E}(\theta)$ and $\Gamma(\theta)$, one can calculate $F_\nu(t)$ from equation (14) by using equations (12) and (13) for the radius $r(\delta, \psi)$ corresponding to arrival time t , and equations (15)–(17) for the factor $\mathcal{F}(\nu, \nu_i)$. In general, the integral in equation (14) must be calculated numerically. To proceed analytically, we obtain an approximate solution to equation (13) by noting that, for small δ , the second term in its left hand side is dominant, while the first term dominates at large δ :

$$\rho \simeq \begin{cases} [(4-s)\tau/\cos \delta]^{1/(4-s)} & \delta < \tilde{\delta} \\ \tau/[2(1 - \cos \delta)\Gamma^2] & \tilde{\delta} < \delta \end{cases}, \quad (18)$$

where $\tilde{\delta}$ is given by $2(1 - \cos \tilde{\delta})\Gamma^2 \rho = [\cos \tilde{\delta}/(4-s)]\rho^{4-s}$. For a relativistic source, most of the radiation received by the

observer comes from a patch of angular size of order $\gamma^{-1} \ll 1$, around the direction toward the observer. In the limit of small angles, $\tilde{\delta}^2 \simeq \rho^{3-s}/[(4-s)\Gamma^2]$, which leads to the following definition of $\tilde{\delta}$:

$$\tilde{\delta} \gamma(\tilde{\delta}, \psi) \simeq (4-s)^{-1/2}. \quad (19)$$

For $\delta < \tilde{\delta}$, equations (2), (3), (12), and (18) lead to

$$r \propto (\mathcal{E}t)^{1/(4-s)}, \quad \gamma \propto \sqrt{[\mathcal{E}t^{-(3-s)}]^{1/(4-s)}}, \quad (20)$$

while for $\tilde{\delta} < \delta$

$$r \propto t/\delta^2, \quad \gamma \propto \delta^{3-s}[\mathcal{E}t^{-(3-s)}]^{1/2}. \quad (21)$$

In both cases the dynamics (i.e. r and γ as functions of observer time) of the ejecta are independent of the initial Lorentz factor Γ . Taking into account that the flux received from the $(d\delta, d\psi)$ patch depends only on r and γ , it implies that this flux is independent of the distribution $\Gamma(\delta, \psi)$ of the initial Lorentz factor across the fireball surface $\Gamma(\delta, \psi)$. Indeed, in either of the above cases, it can be shown explicitly that Γ disappears from the integrand of equation (14). The initial Lorentz factor Γ is relevant only if t is so small that we observe the $(d\delta, d\psi)$ patch before its deceleration begins or before its dynamics becomes adiabatic. Since this is not the case for usual afterglow observations, made at $t \gtrsim 0.1$ days, $\Gamma(\delta, \psi)$ is an irrelevant quantity and will be omitted in following equations.

Returning to the calculation of F_ν , the integral in equation (14) is now approximated as an integral over all directions (δ, ψ) around the observer's line of sight toward the fireball center, satisfying $\delta < \tilde{\delta}$, plus an integral over all directions outside this region. For the simplest case that we shall consider below – observer situated close to the fireball symmetry axis and a decreasing power-law $\mathcal{E}(\theta)$ – the two integrals have the same t -dependence if the fall-off of \mathcal{E} is not too steep, otherwise the $\delta < \tilde{\delta}$ integral is dominant. In such cases, one can obtain analytically the afterglow light-curve decay by retaining only the $\delta < \tilde{\delta}$ integral, which, after substituting $\rho(\tau)$ from equation (18), becomes

$$F_\nu \propto t^{-\frac{6-s}{2(4-s)}} \int_{\Omega[\delta < \tilde{\delta}(t)]} \frac{\delta d\delta d\psi}{(1 + \gamma^2 \delta^2)^3} \mathcal{E}^{[3(2-s) + \frac{6-s}{4-s}]/2(3-s)} \mathcal{F}(\nu, \nu_i), \quad (22)$$

where $\tilde{\delta} \ll 1$ was assumed, so that $\sin \delta \simeq \delta$ and $1 - \beta \cos \delta \simeq (1 + \gamma^2 \delta^2)/(2\gamma^2)$. For the calculation of $\mathcal{F}(\nu, \nu_i)$, equations (15)–(17) give

$$\frac{\nu}{\nu_i} \propto (1 + \gamma^2 \delta^2) \mathcal{E}^{-1/2} t^{3/2}, \quad \frac{\nu_c}{\nu_i} = \mathcal{E}^{[2(s-1) - \frac{4}{4-s}]/(3-s)} t^{4/(4-s)}, \quad (23)$$

thus

$$F_\nu(t) \propto t^{f(p,s)} \int_{\Omega[\delta < \tilde{\delta}(t)]} \frac{\delta d\delta d\psi}{(1 + \gamma^2 \delta^2)^3} [\mathcal{E}(\delta, \psi)]^{g(p,s)}, \quad (24)$$

where the exponents f and g depend on the electron index p and type of external medium.

For the particular case of an observer located on the fireball symmetry axis (i.e. $\theta_{obs} = 0 \rightarrow \theta = \delta$), $\tilde{\delta}$ is defined by

$$\tilde{\delta}^{2(4-s)} [\mathcal{E}(\tilde{\delta})] \propto t^{3-s}. \quad (25)$$

We note that, if the GRB peak flux is correlated with the kinetic energy per solid angle of the ejecta moving along the fireball center – observer line, as expected in the internal and external shock models for GRBs, then we are biased toward localizing and following the afterglows of those GRBs for which we are located within or near regions of the fireball of maximal energy per solid angle. Thus, for an axially symmetric fireball with \mathcal{E} decreasing away from the symmetry axis, it is more likely that we observe predominantly GRBs whose axis is directed nearly toward us.

2.2. Power-Law Fireballs

Hereafter we shall consider fireballs with \mathcal{E} uniform within a core of size θ_c and a power-law outside it:

$$\mathcal{E}(\theta) = \mathcal{E}_0 \times \begin{cases} 1 & \theta < \theta_c \\ (\theta/\theta_c)^{-q} & \theta_c < \theta \end{cases}, \quad (26)$$

with $q > 0$. Other types of structure can be considered as well, but power-laws allow sufficient flexibility with a minimal number of new parameters.

2.2.1. Observers within the Fireball Core

In this case the afterglow light-curve is very close to that for an on-axis observer as illustrated by the off-axis light-curves shown in Granot et al. (2002) for uniform jets. From equation (25)

$$\delta \propto \begin{cases} t^{(3-s)/2(4-s)} & \text{if } \tilde{\delta} < \theta_c \\ t^{(3-s)/[2(4-s)-q]} & \text{if } \theta_c < \tilde{\delta} \end{cases}. \quad (27)$$

$\gamma\delta$ increases with δ , thus $\gamma\delta < \gamma(\tilde{\delta})\tilde{\delta} = (4-s)^{-1/2} < 1$, therefore the denominator in equation (24) can be ignored.

At sufficiently early times, when $\tilde{\delta} < \theta_c$, the observed afterglow emission arises from within the uniform fireball core. In this case, equation (22), together with (11) and (23), yields a decaying light-curve $F_\nu \propto t^{-\alpha_1}$ with

$$\alpha_1 = \begin{cases} (3p-3)/4 & \text{for } s=0 \text{ \& } \nu_i < \nu < \nu_c \\ (3p-2)/4 & \text{for } s=0,2 \text{ \& } \nu_c < \nu_i \\ (3p-1)/4 & \text{for } s=2 \text{ \& } \nu_i < \nu < \nu_c \end{cases}, \quad (28)$$

which are the usual results for a uniform fireball. At later times, when $\tilde{\delta} > \theta_c$, the contribution of the ejecta outside the core to the afterglow emission (eq. [24]) is proportional to

$$\int_{\theta_c}^{\tilde{\delta}} \delta^{1-qg(s)} d\delta = (2 - qg)^{-1} \left(\tilde{\delta}^{2-qg} - \theta_c^{2-qg} \right). \quad (29)$$

For $\tilde{\delta} \gg \theta_c$, this contribution has the same time dependence as that from the fireball core if $qg(s) > 2$, or is dominant if $qg(s) < 2$. Therefore, the asymptotic afterglow light-curve for $\tilde{\delta} > \theta_c$ is $F_\nu \propto t^{-\alpha_2}$ with

$$\alpha_2 = \begin{cases} 3p/4 & (s=0 \text{ \& } \nu < \nu_c) \text{ or } (s=2 \text{ \& } \nu_c < \nu) \\ (3p+1)/4 & (s=0 \text{ \& } \nu_c < \nu) \text{ or } (s=2 \text{ \& } \nu < \nu_c) \end{cases}, \quad (30)$$

if $qg(s) > 2$, while for $qg(s) > 2$

$$(s=0) \quad \alpha_2 = \frac{1}{4 - \frac{1}{2}q} \times \begin{cases} 3p - 3 + \frac{3}{2}q & \nu_i < \nu < \nu_c \\ 3p - 2 + q & \nu_c < \nu \end{cases}, \quad (31)$$

for a homogeneous medium and

$$(s=2) \quad \alpha_2 = \frac{1}{4-q} \times \begin{cases} 3p - 1 - \frac{1}{2}q(p-1) & \nu_i < \nu < \nu_c \\ 3p - 2 - \frac{1}{2}q(p-2) & \nu_c < \nu \end{cases}, \quad (32)$$

for a wind-like medium. Equation (30) applies q larger than

$$\tilde{q} = \begin{cases} 8/(p+4) & (s=0 \& \nu < \nu_c) \text{ or } (s=2 \& \nu_c < \nu) \\ 8/(p+3) & (s=0 \& \nu_c < \nu) \text{ or } (s=2 \& \nu < \nu_c) \end{cases}, \quad (33)$$

while equations (31) and (32) are for $q < \tilde{q}$. Taking into account that for most well-observed afterglows, the electron index is between 1.5 and 2.5, it follows that $5/4 \lesssim \tilde{q} < 7/4$. Therefore, *for fireballs that do not undergo significant lateral spreading at the observing time, the asymptotic index α_2 of the afterglow light-curve is independent of the fireball power-law structure if $q \gtrsim 2$.*

Equations (28) and (30)–(32) allow the calculation of the steepening of the light-curve index $\Delta\alpha = \alpha_2 - \alpha_1$ produced by the passage of the cooling frequency ν_c through observing band or by the core edge becoming visible². For the former, $\Delta\alpha = 1/4$ either if the entire visible region of the fireball is within its core or if the core edge is observable but $q > \tilde{q}$. For $q < \tilde{q}$, the passage of ν_c (which decreases in time for a homogeneous medium, but increases if the medium is wind-like) yields $\Delta\alpha = (2-q)/(8-q) < 1/4$.

The core edge becomes visible at a time t_c when $\gamma\theta_c = 1$. The Lorentz factor of the fluid moving at $\delta = \theta_c$ is given by equation (21) because $\theta_c > \tilde{\delta}$, thus

$$t_c \propto [\mathcal{E}_0\theta_c^{2(4-s)}]^{1/(3-s)}. \quad (34)$$

For $q > \tilde{q}$ the light-curve break across t_c is $\Delta\alpha = 3/4$ for a homogeneous medium and $\Delta\alpha = 1/2$ for a wind, while for $q < \tilde{q}$ the break is

$$\Delta\alpha = \begin{cases} [3q(8\tilde{q}^{-1} - 1)]/[4(8-q)] < 3/4 & s=0 \\ [2q(2\tilde{q}^{-1} - 1)]/[2(4-q)] < 1/2 & s=2 \end{cases}. \quad (35)$$

Therefore the maximal light-curve break that a non-spreading, power-law fireball can yield to an observer located with its uniform core is 3/4 for a homogeneous medium and 1/2 for a wind, being larger for the former.

The light-curve index $\alpha(t) = -(d\ln F_\nu/d\ln t)$ obtained from equation (14) for an on-axis observer is shown in Figure 1 for some values of the structural parameter q . Before the edge core becomes visible, the index $\alpha = \alpha_1$ given by equation (28). When the core edge becomes visible, at $t = t_c \sim 2 \times 10^3 t_d(\theta=0)$ for $s=0$ and $\sim 4 \times 10^3 t_d(\theta=0)$ for $s=2$, the index α increases toward the α_2 given in equations (31) and (32) for $q = 1 < \tilde{q}$ and that given in equation (30) for $q = 2, 3 > \tilde{q}$. As shown in Figure 1, 80% of the light-curve decay steepening across t_c lasts a factor 4–6 in time for $s=0$ and a factor 7–10 for $s=2$. The slower transition for a wind-like medium is caused by the slower decrease of the fireball Lorentz factor with time, given in equations (20) and (21): for $s=0$, $\gamma \propto t^{-3/8}$ if $\delta < \tilde{\delta}$ and $\gamma \propto t^{-3/2}$ if $\delta > \tilde{\delta}$, while for $s=2$, $\gamma \propto t^{-1/4}$ and $\gamma \propto t^{-1/2}$, respectively. The fireball deceleration being slower for a wind-like medium, it takes a longer time for the core edge to become fully visible, thus the transition between the asymptotic light-curve decays is smoother.

²A decelerating source moving at Lorentz factor γ and at an angle δ relative to the direction toward the observer, becomes visible when $\gamma\delta = 1$, so that its emission starts to be relativistically beamed toward the observer.

Figure 1 also shows with continuous lines the light-curve steepening for a fireball with $q = \infty$, corresponding to a uniform, collimated outflow with a sharp edge, that undergoes lateral spreading. Due to the widening of the jet aperture, $\alpha(t < t_c)$ is not constant but increases slowly in time. Furthermore, $\alpha(t \gg t_c)$ is larger than without lateral spreading, reaching the well-known value $\alpha_2 = p$ (Rhoads 1999). For a uniform jet with sideways expansion and interacting with a homogeneous medium, the "fastest" 70% of the analytically expected steepening $\Delta\alpha = p - \alpha_1$, is acquired over a factor 20 in time for $\nu < \nu_c$ and 10 for $\nu_c < \nu$, while for a wind-like medium the corresponding factors are 100 and 1,000, respectively (in the last case, at most 50% of $\Delta\alpha$ can be reached over a factor 100 in time). As we have previously pointed out (Kumar & Panaiteescu 2000), the "jet-break" transition is significantly slower and smoother if the surrounding medium is the wind that a massive GRB progenitor expelled before the burst.

2.2.2. Observers outside the Fireball Core

For observers located outside the uniform fireball core, the pre-break light-curve fall-off is mitigated as the more energetic ejecta located closer to the fireball axis become visible, therefore the early time light-curve index α_1 decreases in time (see also the light-curves presented by Wei & Jin 2003). The fireball axis is seen at a time satisfying

$$t_a \propto [\mathcal{E}_0\theta_{obs}^{2(4-s)}]^{1/(3-s)}, \quad (36)$$

similar to the time t_c when the core edge becomes visible to an on-axis observer (eq. [34]) but with the core size θ_c replaced by the angle θ_{obs} between the fireball axis and the center – observer line (Rossi, Lazzati & Rees 2002). Well after t_a , when the beaming factor \mathcal{D} is almost the same across the fireball core, the light-curve index for an off-core observer should reach that given in equations (30)–(32) for an on-axis observer. Thus, *the flattening of the light-curve fall-off at $t < t_a$ yields larger light-curve breaks $\Delta\alpha$ than for an on-axis observer*. This is the most important feature arising from the structure of the outflow.

Figure 2 shows the evolution of α obtained from equation (14) for an off-core observer located at $\theta_{obs} = 3\theta_c$. As can be noticed, a stronger fall-off of the ejecta energy away from the fireball axis (i.e. a larger parameter q), leads to a more prominent flattening of the afterglow light-curve at $t < t_a$, where $t_a \sim 3 \times 10^3 t_d(\theta=0)$ for $s=0$ and $\sim 10^5 t_d(\theta=0)$ for $s=2$. Also as expected, at $t \gg t_a$ the index α asymptotically reaches the values for an on-axis observer. Note that, for the same parameter q , the light-curve break $\Delta\alpha$ across t_a is larger for a homogeneous medium, and that the transition between the lowest value of α and the α_2 at late time takes about a decade in time for a homogeneous medium and about two decades for a wind-like medium. This indicates that, *for a wind-like stratified medium, light-curve breaks arising from the structure of the outflow may be too shallow compared the light-curve steepenings observed in some afterglows* (see also Granot & Kumar 2003), lasting less than a decade in time.

The minimal value α_{min} reached by the light-curve index before the break depends not only on the structural parameter q , as shown in Figure 2, but also on the location of the observer, through the ratio θ_{obs}/θ_c , and on the slope p of the electron distribution. As illustrated in Figure 3, the observer location has a

much stronger effect on the sharpness of the light-curve break produced by the fireball structure if the external medium is homogeneous. In this case, for observer directions further away from the fireball axis, α_{min} decreases and the transition between α_{min} and the α_2 at late times lasts shorter (relative to the break-time t_a), the light-curve break becoming sharper. Consequently, for a homogeneous medium, higher observer offsets will accommodate easier some of the observed sharp breaks. However, given the expected correlation between the GRB peak flux and the energy of ejecta moving toward the observer, large observer offsets render the burst less likely to be detected. Furthermore, for homogeneous media, as shown in Figure 3, large offsets also yield pre-break light-curve indices that are too small compared to those observed. Taking $\theta_{obs}/\theta_c = 3$ as a more likely case, so that the resulting GRB is sufficiently bright and the afterglow break sufficiently sharp, we show in Figure 4 the dependence of the pre-break minimum light-curve index α_{min} on the structural parameter q and on the electron index p . Because most of the effect of the latter is through the $3p/4$ factor in equation (28), the $\alpha_{min}(q)$ has been offset by its value $\alpha_{min}(q = 0)$ for a uniform fireball, to illustrate the less trivial effect of p on α_{min} .

3. STRUCTURED FIREBALLS/JETS AND AFTERGLOW OBSERVATIONS

The minimum light-curve index α_{min} shown in Figure 2 should be close to the pre-break index usually inferred by fitting the afterglow light-curve with a smoothed broken power-law (e.g. Beuermann et al. 1999), while the post-break index inferred from observations is either the α_2 given in equations (30)–(32) for a structured fireball, or the electron index p for a jet (uniform or with structure) whose edge is visible. Furthermore, one can determine from multiband optical observations the afterglow intrinsic spectral slope β_o , defined as $F_\nu \propto \nu^{-\beta_o}$, which depends only on the electron index p :

$$\beta_o = \begin{cases} (p-1)/2 & \nu_{optical} < \nu_c \\ p/2 & \nu_{optical} > \nu_c \end{cases}. \quad (37)$$

If there is a significant dust reddening in the host galaxy, β_o can be determined with the aid of the X -ray spectral slope, if available, or of fits to the optical spectrum, if it is sufficiently curved to constrain the host extinction for an assumed dust-reddening law (e.g. Jensen et al. 2001, Fynbo et al. 2001). Thus, observations provide three characteristics of the afterglow emission: pre- and post-break light-curve indices α_{min} and α_2 , and spectral slope β_o , which constrain three major fireball parameters: the structural index q , the observer location θ_{obs}/θ_c , and the electron index p .

An analytical determination of q from the measured asymptotic light-curve indices is hampered by the complicated dependence of the pre-break index α_{min} on q and observer location (Figures 2 and 3) and by that the post-break index α_2 could be affected by the lateral spreading of the outflow. The observer location $\theta_{obs} = 3\theta_c$ considered in Figures 2 and 4 can be taken as representative, but, for a more secure approach to determining the fireball structure, one should fit the observed break with a numerically calculated afterglow light-curve, allowing for a free observer location. Before proceeding on this path, we discuss below how the observed asymptotic light-curve indices α_1 and α_2 and the spectral slope β_o can be used to assess if a structured fireball is required by the observations and if the lateral spreading of the outflow is significant.

From equations (28) and (37) it follows that, for a uniform outflow, the pre-break light-curve index is

$$\alpha_1 = \frac{3}{2}\beta_o + \begin{cases} 0 & \text{for } s = 0 \& \nu_i < \nu < \nu_c \\ -1/2 & \text{for } s = 0, 2 \& \nu_c < \nu_i \\ 1/2 & \text{for } s = 2 \& \nu_i < \nu < \nu_c \end{cases}. \quad (38)$$

Thus, if the observed α_1 is smaller than given above, a structured outflow is required (1st criterion), as well as an off-core observer location. Given that for a fireball with a decreasing $\mathcal{E}(\theta)$, the post-break light-curve index α_2 cannot exceed the values given in equation (30), an observed α_2 exceeding

$$\alpha_2 = \frac{3}{2}\beta_o + \begin{cases} 3/4 & \text{for } s = 0 \& \nu < \nu_c \\ 1/4 & \text{for } s = 0 \& \nu_c < \nu \\ 1 & \text{for } s = 2 \& \nu < \nu_c \\ 0 & \text{for } s = 2 \& \nu_c < \nu \end{cases}, \quad (39)$$

requires a collimated outflow whose boundary becomes visible when the light-curve break is observed (2nd criterion). In this case, the post-break light-curve index reaches its maximal value: $\alpha_{max} = p$. From equation (37), it follows that

$$\alpha_{max} = \begin{cases} 2\beta_o + 1 & \nu_i < \nu < \nu_c \\ 2\beta_o & \nu_c < \nu_c \end{cases}. \quad (40)$$

Combining equations (38) and (40), the maximum steepening $\Delta\alpha = \alpha_2 - \alpha_1$ that a uniform jet can produce is

$$\Delta\alpha = \frac{1}{2}\beta_o + \begin{cases} 1 & \text{for } s = 0 \& \nu_i < \nu < \nu_c \\ 1/2 & \text{for } s = 0 \& \nu_c < \nu_i \text{ or } s = 2 \end{cases}. \quad (41)$$

We obtain a 3rd criterion: if the observed $\Delta\alpha$ exceeds the above value, a structured jet is required. However, if the observed α_2 exceeds that given in equation (40), the light-curve break cannot be due entirely to the collimation and the dynamics of the ejecta (4th criterion), implying the existence of another mechanism for light-curve breaks, such as a spectral break passing through the observing frequency band. This passage will also produce a color change and an achromatic light-curve break, which can be detected if observations are done more frequently than the time it takes the spectral break to cross the optical domain.

Applying the above criteria to the features of the optical and X -ray emission of the several afterglows with light-curve breaks, it is possible to identify those cases where structured fireballs or jets are required. Using the 1st criterion above, we find that structured fireballs would be required by the pre-break light-curve indices measured for the optical afterglows 980519, 990123, 991216, and perhaps 000926, if their external media were wind-like (for 990123 and 000926, $\nu_{optical} < \nu_c$ must also be imposed, because X -ray observations do not constrain the location of the cooling frequency). From the 2nd are 3rd criteria above, we find that a uniform jet without structure can accommodate the optical light-curve indices and spectral slope of the afterglows 980519, 990123, 990510, 991216, 000926, and 010222, and that a structured jet would be required by the steepening and post-break light-curve indices of the afterglow 990510 if the medium were a wind, and perhaps for the afterglow 000301c if $\nu_{optical} < \nu_c$. Finally, if $\nu_c < \nu_{optical}$ for the afterglows 991208 and 000301c, the 4th criterion above implies that their steep post-break decays was due to the passage of a spectral feature through the observing band (Li & Chevalier 2001, Panaitescu 2001, Panaitescu & Kumar 2002).

3.1. Numerical Modeling of Structured Jets

Equations (38)–(41) allow one to assess if a structured outflow is required to reproduce the general features of GRB afterglow light-curves, with or without recourse to a significant ejecta collimation and lateral spreading. A more conclusive test should investigate if the light-curve steepening produced by a structured fireball or jet is as sharp as observed, and if the fireball emission at different wavelengths is consistent with the relative intensity of the observed radio, optical, and X -ray fluxes. For uniform outflows, the latter is usually done using a snapshot broadband afterglow spectrum, but, for structured outflows, one has to take in account that the ejecta moving at different angles have different Lorentz factors for the same observer time, thus they radiate at different synchrotron characteristic frequencies.

To perform such a test, the data should be fit numerically, followed by a comparison of the best fit χ^2 obtained for the various model features that are investigated. The model used hereafter is described in our previous work (Panaitescu & Kumar 2000, 2001) on uniform jets. It takes into account the spread in the photon arrival time and Doppler boost due to the curvature of the jet surface, radiative losses, the effect of inverse Compton scatterings on the cooling frequency, and the self-absorption and interstellar scatterings at radio frequencies. The uniform jet is considered to expand sideways at a comoving frame tangential velocity equal to the sound speed c_s , which is calculated from the shock-jump equations and the fireball Lorentz factor. Thus, the jet opening Θ is given by

$$d\Theta(r) = \frac{c_s dt'}{r}, \quad (42)$$

where t' is time measured in the comoving frame. Furthermore, in the uniform jet model, the uniformity is assumed to be maintained during the jet lateral spreading. The variation of the energy per solid angle \mathcal{E} of an infinitesimal ring $(\theta, \theta + d\theta)$ during dt' is $d\mathcal{E} = -\mathcal{E} d(\delta\theta)/\delta\theta$, where $d(\delta\theta)$ is the spreading of the ring during dt' . Therefore, the assumption of jet uniformity at any time is equivalent to that $d(\delta\theta)/\delta\theta$ is a θ -independent quantity. Then, from equation (42), it follows that the spreading of any infinitesimal ring is assumed to be governed by

$$d(\delta\theta) = \frac{\delta\theta}{\Theta} \frac{c_s dt'}{r}. \quad (43)$$

The collimation of ejecta affects the afterglow emission in three ways. First, the size of the visible part of the jet (r/γ) stops increasing when $\gamma\Theta = 1$, i.e. when the edge is seen, yielding a light-curve steepening. Second, the sideways expansion of the jet increases its sweeping area, which alters the jet dynamics. Third, the lateral spreading decreases the surface density of the swept-up medium, moving a fraction of the radiating electrons outside the visible region, if the jet edge is not yet seen. The last two effects are important when $\Theta - \Theta_0 \gtrsim \Theta_0$, Θ_0 being the initial jet opening, which equations (2) and (42) show that occurs slightly *after* the radius where the jet edge becomes visible if the external medium is homogeneous, and slightly *before* if the medium is wind-like. The jet lateral spreading contributes to the light-curve steepening caused by seeing the jet edge, but prolongs the setting in of this steepening more for $s = 2$ than for $s = 0$. For this reason, the light-curve breaks for spreading jets are smoother than those arising from structured fireballs, the effect being stronger for wind-like media than for homogeneous ones (Figures 1 and 2).

That lateral spreading becomes important at about the time when the jet edge is seen, implies that the pre-break afterglow emission for spreading jets is not much affected by the assumed spreading law (eq. [43]). Furthermore, after the lateral spreading becomes important, the jet Lorentz factor falls-off exponentially with radius (Rhoads 1999) for any spreading law involving a constant sideways expansion speed. If this is the sound speed, then it is constant ($c_s = 1/\sqrt{3}$) as long as the jet is relativistic. Therefore, if the jet spreads laterally at a constant speed, then the $F_\nu \propto t^{-p}$ post-break fall-off is not sensitive to the assumed value of that speed, and represents a robust theoretical result.

For a structured jet, we keep the above prescription (eq. [43]) for lateral spreading, but allow for the tangential velocity c_s to vary with the angle θ as resulting from the jet dynamics $\Gamma(\theta)$. Equation (43) provides a simple one-to-one mapping of the jet structure at a time t into that at time $t + dt$, maintaining the numerical algorithm for the jet dynamics computationally inexpensive. We ignore the fluid mixing in the fireball expected to arise from the tangential flow, a factor which Granot & Kumar (2003) have found to have a weak effect on the afterglow emission.

The uniform jet model has six free parameters: the initial energy density per solid angle within the ejecta \mathcal{E} , the jet initial half-opening Θ_0 , the external particle density n (or the parameter A_* introduced by Chevalier & Li 1999 for an r^{-2} wind profile), the exponent p of the electron distribution, and the fractional energies in electrons and magnetic field in the post-shock gas. For observers located within the initial jet opening, this location is irrelevant (Granot et al. 2002). The structured jet model with a power-law distribution of the energy per solid angle has three additional parameters: the core size θ_c , the power-law exponent q , and the observer location θ_{obs} . We apply this model to the 990510 afterglow, with the aim of assessing how much structure is allowed if the external medium is homogeneous, and to test if a wind-like medium can accommodate the observations. We also use the model to investigate if a structured jet can reproduce the steep light-curve break observed in the afterglow 000301c.

3.1.1. GRB 990510

The optical emission of the 990510 afterglow exhibited a break from an index $\alpha_1 = 0.82 \pm 0.02$ to $\alpha_2 = 2.18 \pm 0.05$ (Harrison et al. 1999) at $t \sim 2$ days (see Figure 6). The optical and X -ray slopes, $\beta_o = 0.61 \pm 0.12$ (Stanek et al. 1999) and $\beta_x = 1.03 \pm 0.08$ (Kuulkers et al. 2000), indicate that $\nu_{optical} < \nu_c < \nu_x$.

In the framework of uniform jets, we have previously found (Panaitescu & Kumar 2001) that the optical light-curve steepening can be well accommodated ($\chi^2 = 36$ for 69 degrees of freedom) with a jet of initial kinetic energy $E_0 = (1 \div 6) \times 10^{50}$ ergs, initial opening $\Theta_0 \simeq 3$ deg, interacting with a homogeneous medium of density $n = 0.1 \div 0.4 \text{ cm}^{-3}$. We have also found that a wind-like medium cannot reproduce the steepness of the optical light-curve break, yielding an unacceptable best fit ($\chi^2 = 127$ for 69 df).

For a homogeneous external medium, equation (38) shows that $\alpha_1 = 0.92 \pm 0.18$ for a uniform outflow, which is consistent with the observed index, thus a large structural parameter q is disfavored, otherwise the early decay would be too shallow. Further, equation (39) shows that, for a fireball, the post-break index α_2 cannot exceed 1.67 ± 0.18 , which is too small compared to that observed, thus a spreading jet is re-

quired. In this case, equation (40) leads to a post-break index $\alpha_2 = 2.22 \pm 0.24$, which is consistent with the measured index. The above conclusion that the pre-break light-curve index of the afterglow of GRB 990510 does not allow much structure in a spreading jet is illustrated in Figure 5, showing the χ^2 of the fits obtained for several combinations of the structural parameter q and jet core size-to-opening ratio θ_c/Θ_0 , and for two particular observer locations: the jet axis and the jet edge. By decreasing the θ_c/Θ_0 ratio or increasing q , a stronger jet structure is enforced. As can be noticed, only jets with $\theta_c \gtrsim \Theta_0/5$ provide acceptable fits (defined by a probability larger than 10%), while fits as good as that obtained with a uniform jet ($\chi^2 = 36$) are obtained only for $\theta_c \gtrsim \Theta_0/3$ if $q = 1$ and $\theta_c \gtrsim \Theta_0/2$ if $q = 2$. Therefore, *for a homogeneous external medium, the afterglow of GRB 990510 is best explained by a structured jet with a variation of the energy per solid angle less than a factor 3 across the jet surface*. The radio, optical and X-ray light-curves for the best fit obtained with a structured jet are shown in the left panel of Figure 6. We note that its parameters are similar to those for a uniform jet.

For a wind-like external medium, equation (38) gives $\alpha_1 = 1.42 \pm 0.18$ for a uniform outflow, thus structure is required in this case to explain the slower decay observed at early time. Equation (39) shows that a structured fireball yields $\alpha_2 \leq 1.92 \pm 0.18$, slightly smaller than the observed index, suggesting that collimation may also be required to accommodate the post-break decay of the this afterglow. The right panel of Figure 6 shows the best fit obtained with a structured jet interacting with a wind medium. The structure improves the fit by $\Delta\chi^2 = 23$ relative to the best fit obtained with a uniform jet, which is statistically significant. However, the the optical light-curves steepen too slowly, overestimating the afterglow flux before and after the break and yielding $\chi^2 = 104$ for 66 df. We conclude that *a wind-like medium is not compatible with the observations of the 990510 afterglow even if the jet is endowed with structure*.

3.1.2. GRB 000301c

The *R*-band light-curve index of the 000301c afterglow increased from $\alpha_1 = 0.70 \pm 0.07$ to $\alpha_2 = 2.44 \pm 0.29$ (Bhargavi & Cowsik 2000), with the break occurring at $t \sim 4$ days (Figure 7). Three days after the GRB, Jensen et al. (2001) found that the optical spectral slope is $\beta_o = 0.57 \pm 0.02$ after correcting for the host reddening determined from the curvature of the spectrum, assuming an SMC reddening law. X-ray observations were not made, thus the location of the cooling frequency is not constrained. If $\nu_c < \nu_{optical}$ then the pre-break light-curve index (eq. [38]) $\alpha_1 = 0.36 \pm 0.03$ for a uniform outflow would be too small compared with that observed. Therefore $\nu_{optical} < \nu_c$ seems more likely for the 000301c afterglow.

Given the limitation of structured jets interacting with a wind-like medium to produce sharp light-curve breaks, we focus here only on the model with a homogeneous circumburst medium. For $\nu_{optical} < \nu_c$ and a uniform fireball, equation (38) yields $\alpha_1 = 0.86 \pm 0.03$, slightly larger than observed, thus a structured outflow is only marginally required. For a fireball, equation (39) gives $\alpha_2 \leq 1.61 \pm 0.03$, which is well below the observed value. Thus a jet is required by the post-break steep decay of the 000301c afterglow. Then, according to equation (40), $\alpha_2 = 2.14 \pm 0.04$, which is compatible with the observed decay index measured by Bhargavi & Cowsik (2000). Other post-break asymptotic indices reported in the literature are larger (albeit more uncertain), which suggests that even

a structured jet may have difficulties in reproducing the steep post-break fall-off of the *R*-band light-curve of 000301c.

In the framework of uniform jets, we have found (Panaitescu 2001) that this indeed the case: the best fit obtained with a homogeneous medium has $\chi^2 = 480$ for 98 df and $E_0 \simeq 2 \times 10^{51}$ ergs, $\Theta_0 \simeq 3$ deg, $n \simeq 0.01 \text{ cm}^{-3}$, $p \simeq 2.5$, failing to produce the observed steepening $\Delta\alpha \geq 1.74 \pm 0.30$ when the jet edge becomes visible. For this reason, we have investigated a jet model where the shock-accelerated electron distribution has a break, above which it is steeper, so that the passage through the optical range of the synchrotron characteristic frequency at which the electrons at the break radiate yields the sharp observed light-curve break. Further indication that the distribution of injected electrons is not a pure power-law is provided by the discrepancy between the post-break light-curve indices at radio ($\alpha_r = 1.0 \pm 0.2$) and optical frequencies, and by the change in the *K*–*R* color reported by Rhoads & Fruchter (2001) between 2 and 5 days after the burst. The new best fit obtained with the broken power-law injected electron distribution has $\chi^2 = 120$ for 96 df, being marginally acceptable.

Figure 7 assesses the ability of a structured jet to accommodate the sharp break of the 000301c afterglow without recourse to a non-standard injected electron distribution. The new best fit has $\chi^2 = 204$ for 95 df, which is a substantial improvement in comparison with the uniform jet model and a single power-law electron distribution. Nevertheless, the best fit obtained with a structured jet is not acceptable and, clearly, poorer than the uniform jet model with a broken power-law injected electron distribution. Figure 7 shows that the structured jet model does not reproduced well the shallow decay observed at 8.5 GHz after 50 days and the fall-off seen in the *R*-band light-curve at about the same time. The former is caused by that the post-break light-curve indices at low and high frequencies are not decoupled by the jet structure, an issue which requires a deeper investigation. The latter shortcoming is a more robust result, stemming from that the steepest light-curve fall-off compatible with the spectral slope of the 000301c afterglow (eq. [40]) is smaller than the observed post-break index α_2 . We note that, in the best fit obtained with a structured jet, the cooling frequency falls within the optical domain at a few days, a feature which is required to explain the observed curvature of the optical spectrum (Jensen et al. 2001) and reddening of the optical afterglow emission (Rhoads & Fruchter 2001).

4. CONCLUSIONS

In the standard picture of uniform jets, the measured pre- and post-break light-curve indices and the spectral slope offer an overconstrained problem, as all these quantities depend only on the exponent of the power-law distribution of shock-accelerated electrons. For the purpose of testing the fireball model and of determining various afterglow physical parameters, the most important feature brought in by the angular structure of GRB jets is the diversity of light-curve decay indices (eq. [30]–[32], Figures 2–4). For most (if not all) well-observed afterglows, one can identify a type of external medium, location of cooling frequency, and geometry of ejecta that account for the observed light-curve indices and spectral slopes, indicating that the freedom allowed by the outflow structure is usually not required by current afterglow observations. Indeed, using an uniform jet model, we have previously found (Panaitescu & Kumar 2002) good fits for the afterglows 980519, 990123, 990510, 991208, 991216, 000301c, 000418, and a marginally acceptable fit for 000926. Nevertheless, a simple analysis of the measured light-

curve indices and spectral slopes, presented in §3, shows that structured outflows is required if the circumburst medium has a wind-like profile. The reason is that wind-like media yield steeper light-curve decays, so that for the electron index p constrained by the optical spectral slope, structure in the outflow is required to explain the shallower light-curve fall-off that is observed.

In our previous work on the light-curves of collimated GRB ejecta (Kumar & Panaiteescu 2000), we have shown that a circumburst medium with a wind-like stratification yields a light-curve break that is too smooth compared with observations. Given that a structured outflow can produce a shallower light-curve decay before the break, it is worth investigating if angular structure allows wind-like media to be consistent with the observations. Figures 2 and 3 show that it takes more than a decade in time to the light-curves for wind-like media to acquire most of the steepening. This property arises from the slower evolution of the fireball Lorentz factor and the stronger sideways expansion when the jet edge becomes visible, and indicates that even structured jets interacting with a wind-like medium may have a serious problem in accommodating the observations. This shortcoming of stratified circumburst media to produce sufficiently sharp breaks is illustrated in the right panel of Figure 6.

The ability of structured jets to yield larger light-curve breaks was also employed to test if a broken power-law injected electron distribution is really required to explain the strong break

observed in the R -band light-curve of the 000301c afterglow. In §3.1.2 find that, although the addition of structure greatly improves the quality of the fit obtained with a pure power-law electron distribution, it does not fare as well as a jet model with a non-standard, broken power-law electron distribution. In part, this is due to the shallower than observed fall-off of the post-break light-curve produced by a structured jet (Figure 7) for the electron index p required by the slope of the optical spectrum.

Using numerical calculations of the dynamics and synchrotron emission of structure jets, we have also shown (§3.1.1) that, for the afterglow 990510, not much angular structure is allowed by observations. Although acceptable fits can be obtained even with a tenfold variation of the energy per solid angle within the jet, fits of quality comparable to that obtained with a uniform jet require an energy variation across the jet surface of less than a factor 3. A stronger angular structure in the ejecta may, however, be allowed for other GRB afterglows. Evidently, the best cases for a structured outflow will be those where the light-curve indices and spectral slopes are not consistent with each other within the framework of uniform fireballs. In such cases, equations (38)–(40) and the criteria derived in §3 offer a simple way to assess the importance of structure and collimation in the outflow, for a well-measured optical spectral slope. Furthermore, equations (28), (30)–(32), and the results shown in Figure 5, can be used to constrain the type of the power-law distribution of the ejecta kinetic energy with the off-axis angle.

REFERENCES

Beuermann, K. et al. 1999, A&A 352, L26
 Bhargavi, S. & Cowsik, R. 2000, ApJ 545, L77
 Chevalier, R. & Li, Z.-Y. 1999, ApJ 520, L29
 Frail, D. et al. 2001, ApJ 562, L55
 Fynbo, J. et al. 2001, A&A 373, 796
 Granot, J. et al. 2002, ApJ 570, L61
 Granot, J. & Kumar, P. 2003, ApJ, submitted (astro-ph/0212540)
 Harrison, F. et al. 1999, ApJ 523, L121
 Jensen, B. et al. 2001, A&A 370, 909
 Kardashev, N. 1962, AJ 6, no.3, 317
 Kumar, P. & Panaiteescu, A. 2000, ApJ 541, L9
 Kuulkers, E. et al. 2000, ApJ 538, 638
 Li, Z.-Y. & Chevalier, R. 2001, ApJ 551, 940
 Mészáros, P., Rees, M.J. 1997, ApJ 476, 232
 Mészáros, P., Rees, M.J. & Wijers, R. 1998, ApJ 499, 301
 Panaiteescu, A. & Kumar, P. 2000, ApJ 543, 66
 Panaiteescu, A. & Kumar, P. 2001, ApJ 554, 667
 Panaiteescu, A. 2001, ApJ 556, 1002
 Panaiteescu, A. & Kumar, P. 2002, ApJ 571, 779
 Postnov, K., Prokhorov, M. & Lipunov, V. 2001, Astronomy Report 45, 236 (astro-ph/9908136)
 Rhoads, J. 1999, ApJ 525, 737
 Rhoads, J. & Fruchter, A. 2001, ApJ 546, 117
 Rossi, E., Lazzati, D. & Rees, M.J. 2002, MNRAS 332, 945
 Stanek, K. et al. 1999, ApJ 522, L39
 Wei, D. & Jin, Z. 2003, A&A, submitted (astro-ph/0212514)
 Zhang, B. & Mészáros, P. 2002, ApJ 571, 876

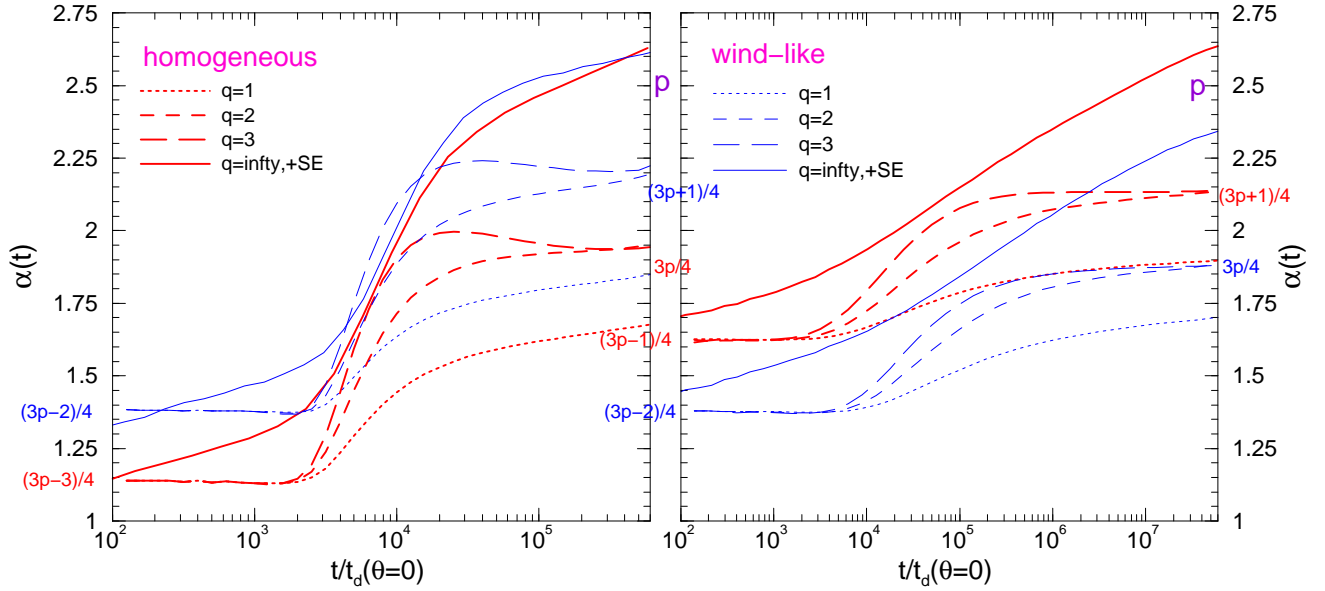


FIG. 1.— Evolution of the logarithmic derivative $\alpha = -(d \ln F_\nu / d \ln t)$ of the afterglow flux at frequencies below and above the cooling frequency (thin and thick curves, respectively), for homogeneous (left panel) and wind-like (right panel), and for a few values of the parameter q for the assumed power-law dependence of the energy per solid angle \mathcal{E} on the angle θ measured from the symmetry axis of the fireball: $\mathcal{E}(\theta) \propto \theta^{-q}$. Close to the fireball axis, $\mathcal{E}(\theta)$ is assumed constant. Solid curves are for a uniform jet with sharp boundaries (corresponding to $q = \infty$) and undergoing sideways expansion. The electron distribution injected in the shocked gas is taken to be a power-law of exponent $-p$ with $p = 2.5$. The observer is placed on the fireball axis, the observer time being measured in units of the deceleration timescale of the gas moving along the fireball axis. The asymptotic light-curve indices at early and late times are indicated on the abscissa. Note the faster transition between the asymptotic indices in the case of a homogeneous medium, and that, for $q \geq 2$, α_2 is independent of q , as the afterglow emission arises mostly from the fireball core.

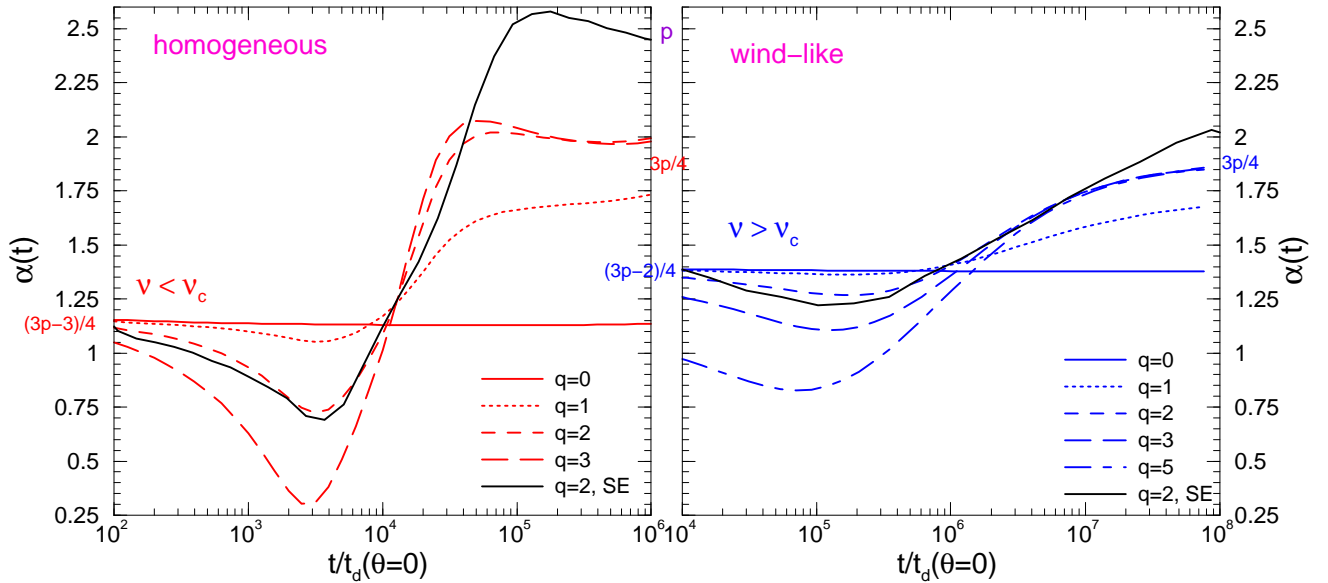


FIG. 2.— Evolution of the light-curve index for various parameters q for the power-law fireball structure and an observer located at an angle $\theta_{obs} = 3\theta_c$ relative to the symmetry axis of the fireball, θ_c being the angular size of fireball uniform core. The electron distribution parameter is $p = 2.5$. When the fireball has decelerated enough that its core becomes visible, the light-curve index α has a minimal value that depends on q and on the ratio θ_{obs}/θ_c . Note the slower evolution of α for a wind-like medium and the weaker effect that the jet structure has on α in this case. In the cases not shown ($\nu > \nu_c$ for a homogeneous medium and $\nu < \nu_c$ for a wind), the evolution of α is similar, the curves being shifted upward by $1/4$. The continuous black line is for a $q = 2$ jet undergoing lateral spreading and for an observer located on the jet edge at $t = 0$, i.e. the jet opening initial opening is $\Theta_0 = 3\theta_c$.

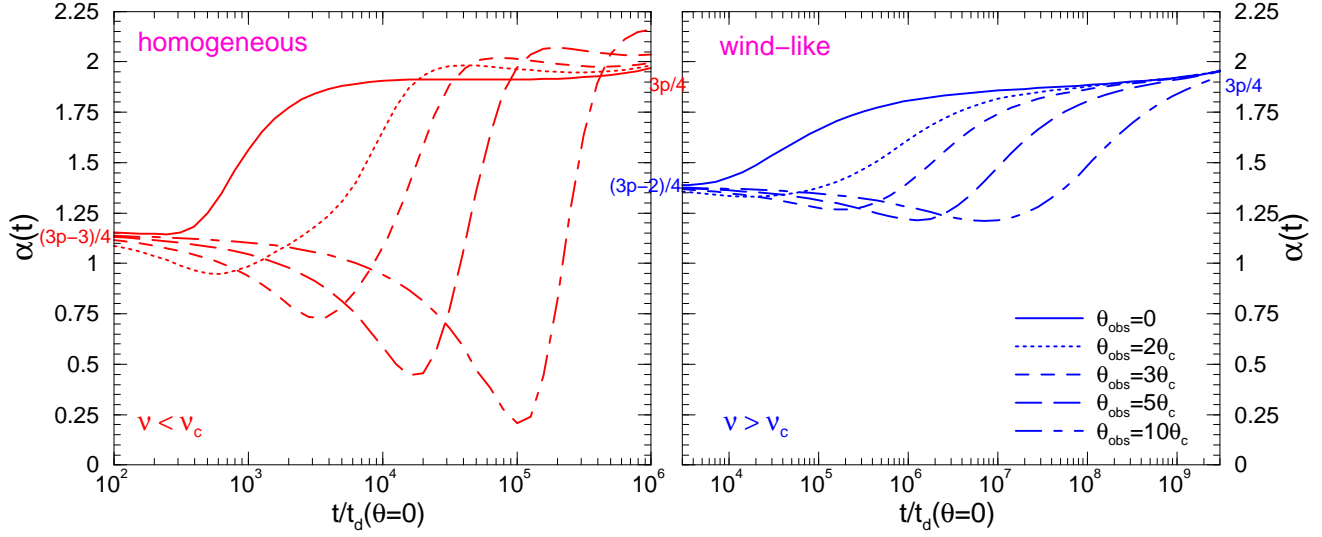


FIG. 3.— Same as in Figure 2 but for a fixed parameter $q = 2$ and various ratios θ_{obs}/θ_c . The line coding is the same for both panels. Note that observers located further away from the fireball symmetry axis will see a stronger flattening of the afterglow light-curve followed by a sharper break, and that the break is shallower for a wind-like medium.

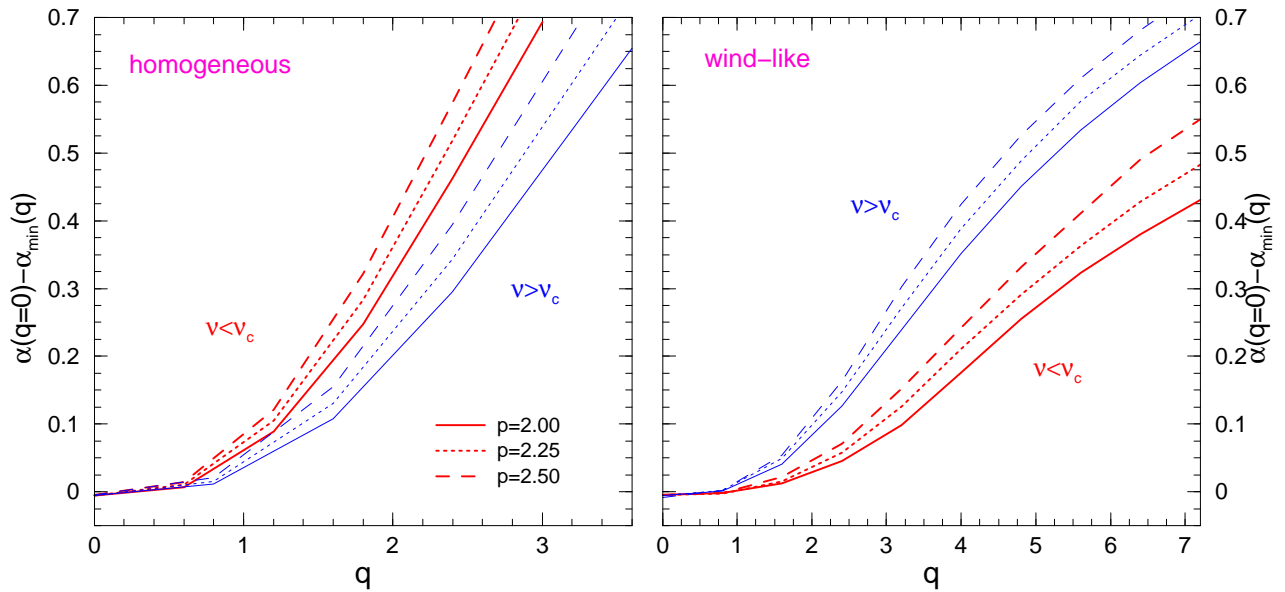


FIG. 4.— Effect of fireball structure (parameterized by q) on the minimum light-curve index α_{min} reached before the break, for a few values of the electron index p (solid curves: $p = 2$, dotted curves: $p = 2.25$, dashed curves: $p = 2.5$). The observer location is $\theta_{obs} = 3\theta_c$. Thick curves are for $\nu < \nu_c$, while thin lines indicate $\nu > \nu_c$. Most of the dependence of α_{min} on p has been eliminated by shifting vertically the curves by the $\alpha(q = 0)$ expected for a uniform fireball. Note the stronger flattening (i.e. decrease of α_{min}) that a homogeneous medium yields for the same structural parameter q .

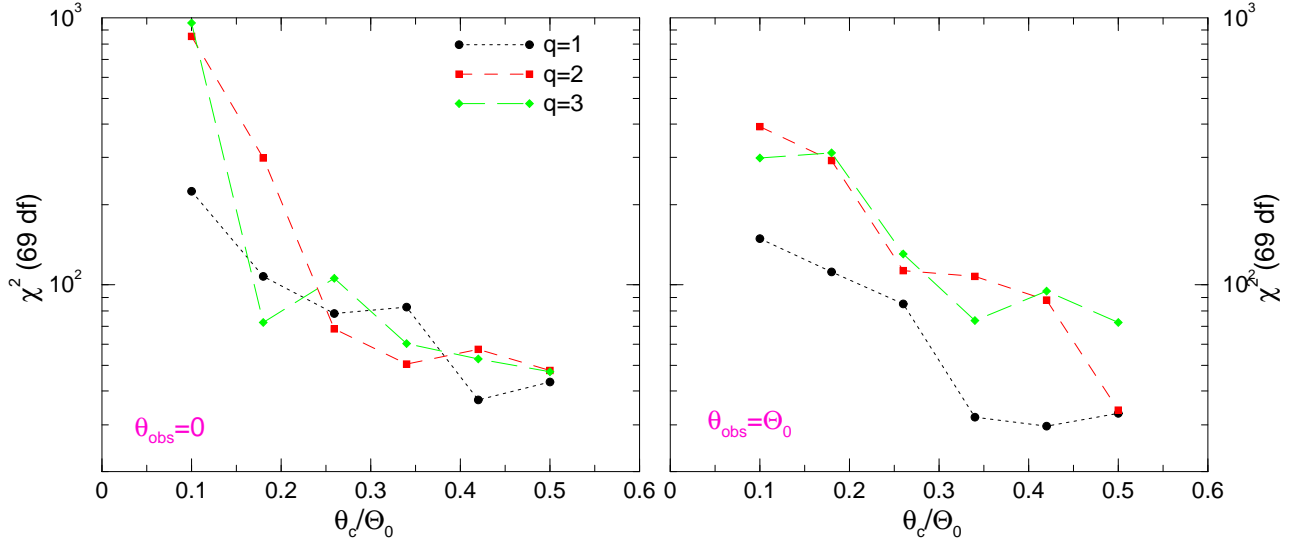


FIG. 5.— Variation of the χ^2 of the best fits to the radio, optical, and X -ray emission (75 data points, 69 degrees of freedom) of the 990510 afterglow, with the amount of structure in the spreading jet. Left panel: observer on jet axis, right panel: observer on edge axis. Each point represents a combination of jet core size-to-opening ratio θ_c/Θ_0 and exponent q of the power-law jet structure (see §3 for other model parameters, which were left free). Note that, as the angular distribution of the jet energy is more anisotropic, the fits become poorer. The best fit obtained with a uniform jet has $\chi^2 = 36$. Fits of comparable quality require a variation of the energy per solid angle of less than a factor 3 across the jet surface.

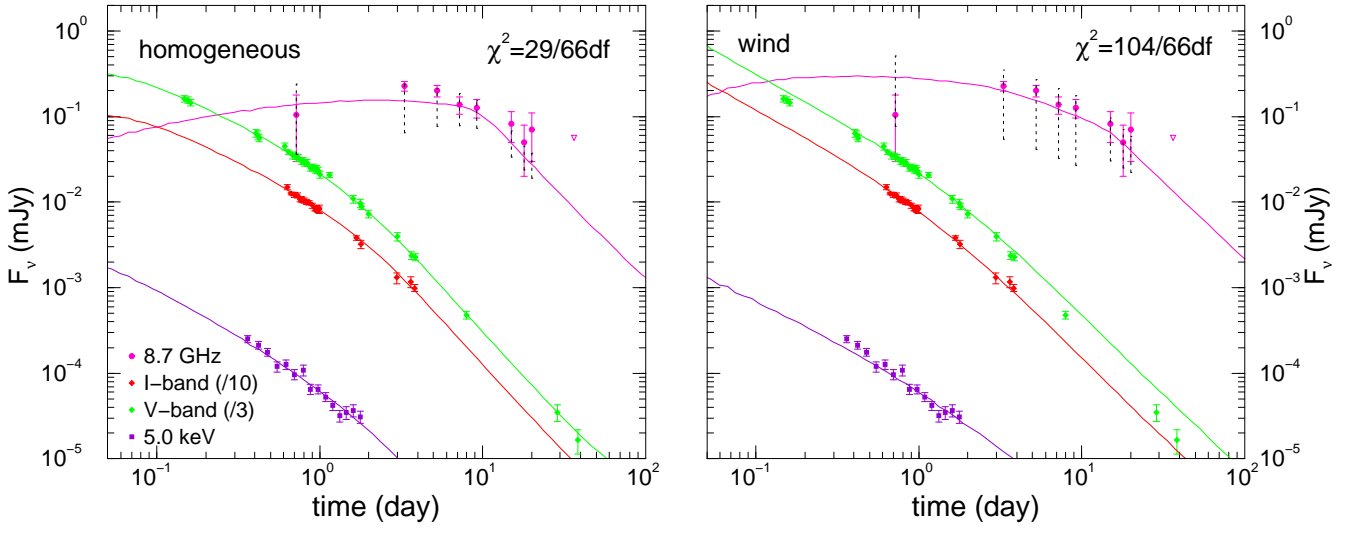


FIG. 6.— Best fits for the 990510 afterglow obtained with structured jets interacting with a homogeneous (left panel) and wind external media (right panel). Left panel – the jet parameters are: initial energy density per solid angle along the jet axis $\mathcal{E}_0 \simeq 10^{53}$ ergs/sr, initial jet half-opening $\Theta_0 \simeq 2.2\theta_c$, observer location $\theta_{obs} \simeq 2.2\theta_c$, size of jet uniform core $\theta_c \simeq 0.8$ deg, exponent of power-law angular distribution of energy within the jet $q \simeq 1.5$ (thus the initial energy of the jet is $E_0 \simeq 2 \times 10^{50}$ ergs), electron index $p \simeq 1.8$, and external density $n \simeq 0.2 \text{ cm}^{-3}$, yielding $\chi^2 = 29$ for 66 degrees of freedom (df). Right panel: $\mathcal{E}_0 \simeq 8 \times 10^{52}$ ergs/sr, $\Theta_0 \simeq 4.6\theta_c$, $\theta_{obs} \simeq 1.8\theta_c$, $\theta_c \simeq 1$ deg, $q = 2 \div 3$ (therefore $E_0 \lesssim 3 \times 10^{50}$ ergs), $p \simeq 1.8$, and wind parameter $A_* \simeq 0.2$, yielding $\chi^2 = 104$ for 66 df. In both cases, the cooling frequency falls in the optical range, the spectral slope being in between the values given in equation (37). The vertical dotted lines indicate the amplitude of the fluctuations at 9 GHz caused by inhomogeneities in the Galactic interstellar medium in the direction of GRB 990510. For clarity, the optical fluxes have been shifted by the factors indicated in the legend. Note that, for a wind-like medium, the steepening of the light-curve is too slow, failing to accommodate the sharpness of the break seen at 2-3 days.

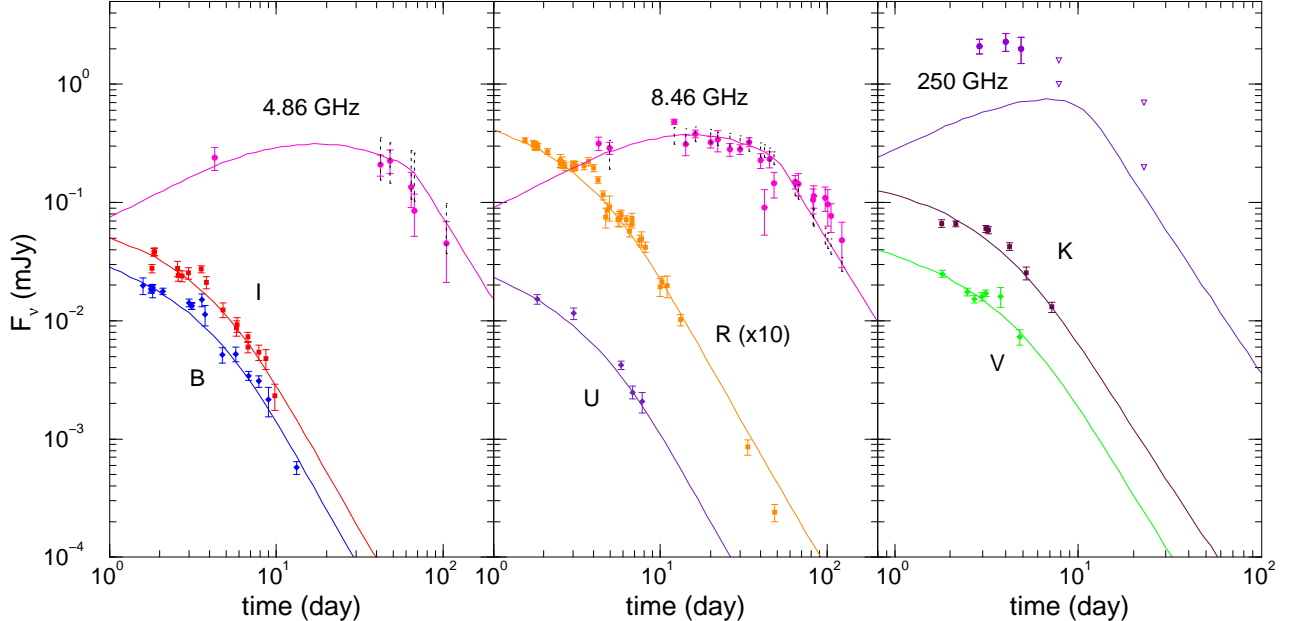


FIG. 7.— Best fit for the 000301c afterglow obtained with a structured jet and a homogeneous external medium. The jet parameters are $\mathcal{E}_0 \simeq 3 \times 10^{53}$ ergs/sr, $\Theta_0 \simeq 5.8 \theta_c$, $\theta_{obs} \simeq 3.8 \theta_c$, $\theta_c \simeq 0.7$ deg, $q \sim 3$ (therefore $E_0 \sim 3 \times 10^{50}$ ergs), $p \simeq 2.5$, and $n \simeq 0.04 \text{ cm}^{-3}$. The jet energy is 6 times smaller than that obtained with a uniform jet, while the density is 4 times larger. This fit has $\chi^2 = 204$ for 95 df, excluding the data between 3.0 and 4.3 days, when the optical emission exhibited a flattening indicating a departure (e.g. delayed energy injection, clumpy external medium) from the jet model used here. This anomalous feature is simultaneous with the optical light-curve break. Note the steeper than observed fall-off the 8.5 GHz emission after 50 days, and the too shallow decay of the *R*-band emission at late times. Triangles indicate 1σ and 2σ upper limits for the 250 GHz emission. As for Figure 6, vertical dotted lines give the amplitude of interstellar scintillation at radio frequencies.